

# Spectroscopic Investigation of Bianthryl-Based Metal–Organic Framework Thin Films and Their Photoinduced Topotactic Transformation

Zeinab Mohammed Hassan, Peter G. Weidler, Alexei Nefedov, Yi Luo, Stefan Heißler, Manuel Tsotsalas, Ritesh Haldar,\* and Christof Wöll\*

Metal–organic frameworks (MOFs) have gained a large amount of interest because of their periodic and modular structure. These features allow easy prediction of the physical and chemical properties of an organic chromophore, acting as a linker in the MOF. In the present work, a bianthryl (BA) chromophore, equipped with metal-coordinating carboxylate groups, is studied to construct a photoluminescent Zn-BA surface-anchored MOF (SURMOF) thin film. The Zn-BA SURMOF, in response to prolonged UV light irradiation under ambient conditions, exhibits prominent changes in the ground and excited state optical properties, without losing its crystalline structure. A detailed spectroscopic study using UV–vis, infra-red, Raman, and electron paramagnetic resonance (EPR) reveals that in the presence of O<sub>2</sub> a photoinduced topotactic transformation is initiated by the formation of singlet oxygen, which then reacts with the BA linkers to form endoperoxide.

large number of MOF structures (>100 000) till date. The large chemical space in the MOF materials allows realizing a variety of different chemical and physical properties by straightforward variation of node-linker combinations. The structural periodicity and isorecticular synthesis<sup>[3]</sup> strategies aided by and using computational methods have allowed us to preconceive numerous materials targeted for specific applications. These remarkable features of MOFs have created great promise for applications in gas storage and separation,<sup>[4–5]</sup> catalysis,<sup>[6]</sup> sensing,<sup>[7–8]</sup> and optoelectronics.<sup>[9–10]</sup>

With regard to device integration, bulk powder MOFs synthesized via conventional solvothermal methods are not always suitable.<sup>[11]</sup> Deposition of powder

materials on solid substrates typically results in films with heterogeneous morphology, weak adhesion to the support, and high defect densities. Among the thin film fabrication methods, the layer-by-layer (lbl), liquid-phase epitaxy (LPE) method that allows growing surface-anchored MOF thin films (SURMOFs) on appropriately functionalized substrates has been found to be particularly useful. This approach allows fabricating monolithic thin films with reduced defect density.<sup>[12]</sup> In particular, for optical and electronic applications, the SURMOF approach has striking advantages because of an enhanced light penetration depth into the material, straightforward deposition on conductive and transparent substrates, and easy photophysical characterization, e.g., using transient absorption spectroscopy.<sup>[13]</sup>

MOFs allow for a predictable and straightforward assembly of organic chromophores into crystalline arrays with high structural order. Consequently, this approach has been successfully used to study photophysical properties of light-responsive chromophoric MOFs.<sup>[13–14]</sup> Organic dyes and semiconductors, such as porphyrins,<sup>[15–17]</sup> phthalocyanines,<sup>[18–19]</sup> naphthalene/perylene-diimides,<sup>[20–22]</sup> pentacene,<sup>[23]</sup> anthracene,<sup>[24]</sup> perylene,<sup>[25]</sup> and other similar chromophores, have been successfully assembled into MOFs and MOF thin films. In many cases, the photoexcited and charge separated states in these MOFs have been explored for various applications involving light emission, photovoltaics, and nonlinear optics.<sup>[26–29]</sup> Instead of electronic excitation, absorption of light can also lead to chemical changes under ambient condition.<sup>[30–33]</sup> So far, the photochemistry of MOFs and SURMOFs has received only little attention. In particular, in the presence of ambient

## 1. Introduction

Metal–organic frameworks (MOFs) are a class of crystalline, intrinsically porous materials formed by linkage of metal/metal-oxo nodes with suitably functionalized organic linkers.<sup>[1–2]</sup> Virtually infinite possibilities of the node-linker combinations have resulted in a

Z. M. Hassan, P. G. Weidler, A. Nefedov, Y. Luo, S. Heißler, M. Tsotsalas, R. Haldar, C. Wöll

Institute of Functional Interfaces (IFG)  
Karlsruhe Institute of Technology (KIT)  
Hermann-von Helmholtz-Platz 1, 76344 Eggenstein-Leopoldshafen,  
Germany  
E-mail: christof.woell@kit.edu

Z. M. Hassan  
Chemistry Department  
Faculty of Science  
Fayoum University  
P.O. Box 63514, Fayoum 63514, Egypt

R. Haldar  
Tata Institute of Fundamental Research Hyderabad  
Gopanally, Hyderabad, Telangana 500046, India  
E-mail: riteshaldar@tifrh.res.in

 The ORCID identification number(s) for the author(s) of this article can be found under <https://doi.org/10.1002/admi.202102441>.

© 2022 The Authors. Advanced Materials Interfaces published by Wiley-VCH GmbH. This is an open access article under the terms of the Creative Commons Attribution License, which permits use, distribution and reproduction in any medium, provided the original work is properly cited.

DOI: 10.1002/admi.202102441

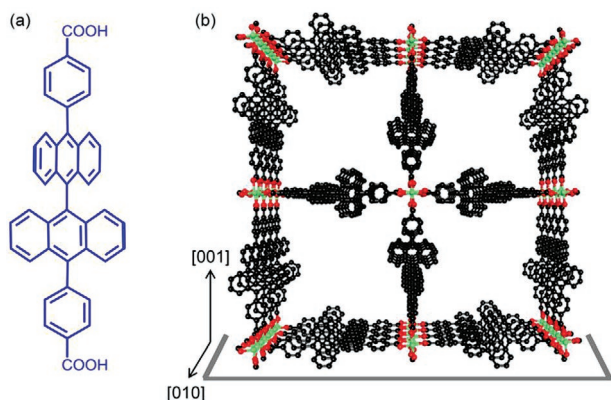


**Figure 1.** a) Chemical structure of the BA-linker; b) Illustration of the oriented Zn-BA SURMOF-2.

$O_2$  and moisture ( $H_2O$ ) photoexcitation can lead to new chemical product formation, which may change the photophysical properties of the chromophoric MOF under investigation. Such photo-induced chemical changes are difficult to predict and can render new properties to the molecular assemblies. Importantly, cooperative effects may result in pronounced differences to the photochemistry of the individual solvated chromophores.

In the present work, the SURMOF approach has been used to assemble an organic chromophoric linker, bianthryl (BA), into a crystalline array. BA, composed of two anthracene rings positioned in an orthogonal geometry, has been studied in quite some detail due to its interesting excited-state photophysics.<sup>[34–35]</sup> As a result of a photo-induced rotation around the C–C axis (Figure 1a), the ground and excited state geometries of the BA molecule are very different.<sup>[36]</sup> Experimental investigations of these excited states are difficult to carry out in the solvated state since interactions with solvent molecules result in severe complications. In addition to solvatochromic effects, the quenching of the excited states and the steric constraints imposed by the (disordered) solvation shell have to be considered.<sup>[36]</sup> Incorporation of this twisted BA as linker in the crystalline, porous MOF structure removes any solvatochromic effects. The rotational freedom of the chromophore is reduced compared to the solvated molecule, but the crystalline environments allow studying the effects of this steric constraint in a much more systematic fashion. For

example, in previous work on the photoswitching of azobenzene side groups embedded in a SURMOF, theoretical approaches could be used to identify—by studying in detail the trajectory of the outer phenyl group during the isomerization process—the reasons for the absence of switching when the linker length was too short.<sup>[37]</sup> Extending the length of the linker then allowed us to reversibly switch the sidegroups between the cis- and the trans conformation, allowing for interesting applications in the controlled release of molecules.<sup>[38]</sup>

In this work, we have used the lbl method to realize a well-defined 3D assembly of BA in a Zn-SURMOF-2 type structure. In this crystalline framework, the BA-linkers are arranged in a close-packed geometry, as shown in Figure 1. Upon prolonged irradiation with UV light (365 nm) under ambient conditions, we observed that the Zn-BA SURMOF-2 undergoes an irreversible change without losing the structural order. An in-depth spectroscopic characterization, employing UV-vis, infra-red, Raman, EPR, and Near-Edge X-ray Absorption Fine Structure (NEXAFS) spectroscopy, revealed an oxidation process involving one of the anthracene rings of BA and singlet oxygen ( $^1O_2$ ). In the following, we illustrate the sensitization process of  $^1O_2$  by the Zn-BA SURMOF and the consequent photochemical reaction, yielding a stable peroxide-functionalized SURMOF.

## 2. Results and Discussion

A SURMOF-2 type structure is formed by connecting ditopic organic linker and paddle-wheel type secondary building unit (SBU) of Zn or Cu-O cluster, as shown in Figure 1b.<sup>[39]</sup> The 2D squares formed by this linkages, further stack along [010] direction to yield an oriented 3D structure. To confirm the SURMOF-2 type structure of the Zn-BA thin film, out-of-plane and in-plane X-ray diffraction measurements were carried out (Figure 2a). The out-of-plane XRD pattern revealed (001) reflexes, while the in-plane XRD pattern exhibited (100) reflexes, suggesting an oriented growth of the Zn-BA SURMOF-2 type structure with the [001]-direction oriented perpendicular to the substrate plane. From the positions of the XRD peaks we concluded unit cell parameters of  $a = b = 2.7$  nm. The (010) diffraction peak observed in the in-plane XRD pattern suggested an inter-2D plane distance (lattice parameter  $b$ ) of 6.5 Å.

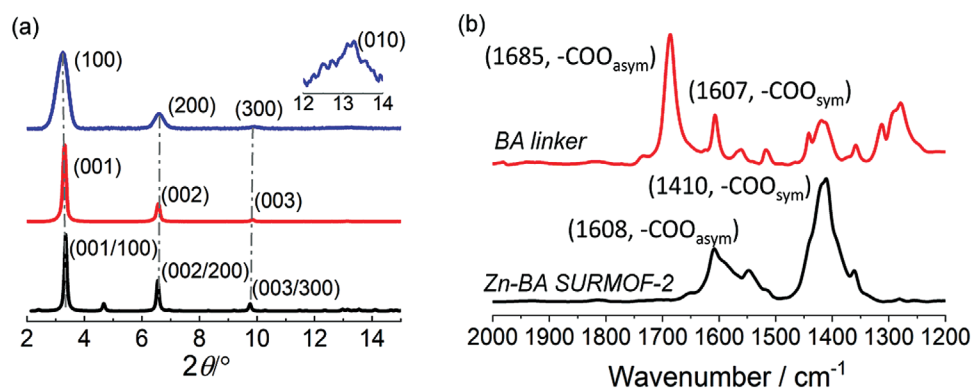


**Figure 2.** a) Simulated (black), experimental out- (red) and in-plane (blue) XRD patterns of the Zn-BA SURMOF-2; b) IR spectra of the BA linker and the Zn-BA SURMOF-2.

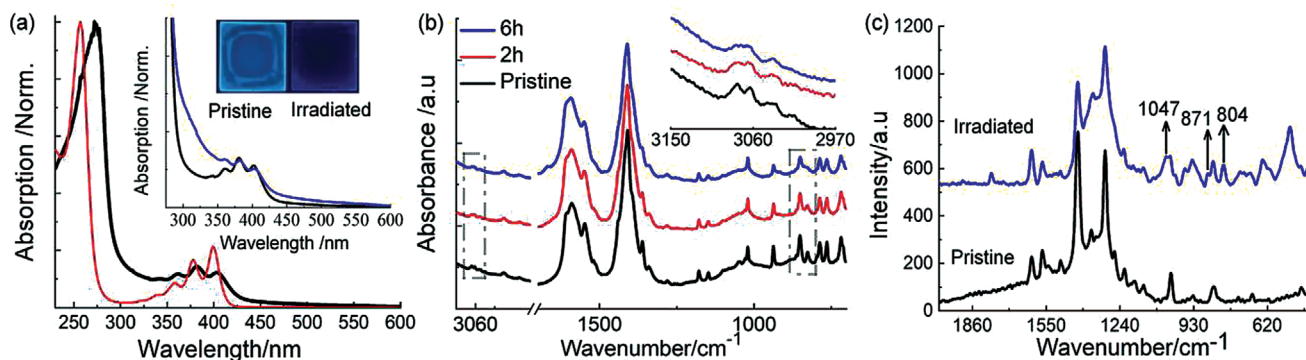


**Figure 3.** a) UV-vis spectra of the BA linker (red) and pristine Zn-BA-SURMOF (black), Inset: UV-vis spectra of the pristine and irradiated (blue) Zn-BA-SURMOF, photograph of the pristine and irradiated Zn-BA SURMOF under UV light; b) IRRAS spectra for Zn-BA-SURMOF in pristine and irradiated form; c) Raman spectra of the Zn-BA SURMOF, before and after irradiation.

IRRAS measurement of Zn-BA thin film further confirmed the presence of Zn-paddle-wheel type SBUs, key to the Zn-SURMOF-2 structure, by exhibiting characteristic  $\text{COO}^-$  symmetric and asymmetric stretching bands at 1608 and 1410  $\text{cm}^{-1}$ , respectively (Figure 2b).

The two anthracene units in the BA linker are rotated out-of-plane, and hence no conjugation between the two anthracene moieties should be present. This absence of direct electronic coupling is evidenced by the UV-Vis spectrum recorded for BA dissolved in ethanol. The spectrum clearly exhibits vibronically resolved  $\pi-\pi^*$  transitions with the lowest energy transition at 399 nm (Figure 3a), very similar to the absorption spectrum observed for single anthracene molecules.<sup>[40]</sup> After assembly into the SURMOF-2 structure, the absorption spectrum exhibited slightly red shifted lowest energy transition at  $\approx 405$  nm, and the vibronic intensities changed compared to the solvated BA molecule, as shown in Figure 3a. This observation indicates that the anthracene units of the BA linker interact along the stacking direction, i.e., the [010] axis, as expected from the short distance between the 2D layers. Further, the broad emission spectrum observed for Zn-BA upon excitation at 375 nm suggested anthracene excimer state emission, confirming the presence of inter-BA linker interaction, as shown in Figure S6 (Supporting Information).

To our surprise, we observed a very distinct change in the Zn-BA UV-Vis spectrum upon prolonged exposure to UV light (365 nm, 6 h, 51  $\text{mW cm}^{-2}$ ) under ambient conditions. Illumination caused a strong enhancement of the absorption at  $\approx 315$  and 440 nm, accompanied by a strong reduction in the emission intensity, as shown in Figure 3a, inset. Keeping the thin film in the dark for longer periods of time did not bring back the original absorption spectrum, indicating an irreversible change. These changes, however, did not occur in  $\text{O}_2$ -free environment, indicating a photochemical transformation of the Zn-BA thin film involving  $\text{O}_2$ , as indicated in Figure S7 (Supporting Information).

To understand these photoinduced changes, we performed the following experiments. First, we studied the BA-linker in solution. In tetrahydrofuran (THF), BA exhibited changes in the absorption spectra, similar to those observed for Zn-BA film. This confirmed that the changes observed in the Zn-BA film correspond to the BA-linker, as indicated in Figure S8 (Supporting Information). Next, we investigated whether the

photochemical change also affects the crystallinity. Under continuous UV-light illumination, out-of-plane and in-plane XRD patterns were recorded. After  $\approx 10$  h of photoreaction, the XRD patterns did not change substantially along the [001] and [100] directions, as shown in Figure S9 (Supporting Information). This observation suggests that the crystallinity of the Zn-BA structure remained intact during the photochemical transformation. In addition, also the morphology of the film did not change upon irradiation, as evidenced by scanning electron microscopy images in Figure S10 (Supporting Information).

NEXAFS spectroscopy is very sensitive to an occupation of lowest unoccupied molecular orbitals (LUMO) that allows understanding the change in the electronic structure of Zn-BA SURMOF after the irradiation. NEXAFS spectra ( $\pi^*$ -resonance region) recorded at the carbon K-edge of Zn-BA before (black) and after UV-light irradiation (red) is shown in Figure S11 (Supporting Information). The observed peaks at photon energies of 284.5, 284.9, and 285.5 eV correspond to resonant electron transitions from C1s core level to LUMO, LUMO+1, and LUMO+2 levels, respectively. From Figure S11 (Supporting Information), it is evident that these peak intensities are reduced after the UV-light irradiation. This could be explained as filling of the LUMO orbitals resulting from the oxidation of BA linker.

To obtain detailed insight into the specific changes of the Zn-BA structure, we carried out infrared and Raman spectroscopy measurements. The IRRAS data for the UV-light irradiated Zn-BA film in an ambient atmosphere for 2 and 6 h revealed that the  $\text{COO}^-$  asymmetric and symmetric stretching modes of the Zn-paddlewheel ( $\text{Zn}_2(\text{COO})_4$ ) node remain unchanged, compared to the pristine Zn-BA (Figure 3b). This suggests that the photoirradiation did not affect the metal-coordination environment. However, the absorbance intensities of the bands around 3100 and 830-810  $\text{cm}^{-1}$  (marked in gray box, Figure 3b), which correspond to aromatic  $\text{C}=\text{C}$ - stretching and bending, respectively, decreased with increasing time of irradiation. Involvement of the aromatic  $\text{C}=\text{C}$ - bonds in the anthracene units suggests the formation of an oxidized product, formed between the anthracene and reactive molecular oxygen species ( $^1\text{O}_2$ ). Since the most likely addition product (endoperoxide), includes IR silent  $\text{-O-O-}$  group, we also recorded Raman spectra of the irradiated Zn-BA films. The irradiated Zn-BA thin film exhibited new bands at 803.5  $\text{cm}^{-1}$  (strong), 870  $\text{cm}^{-1}$  (medium),

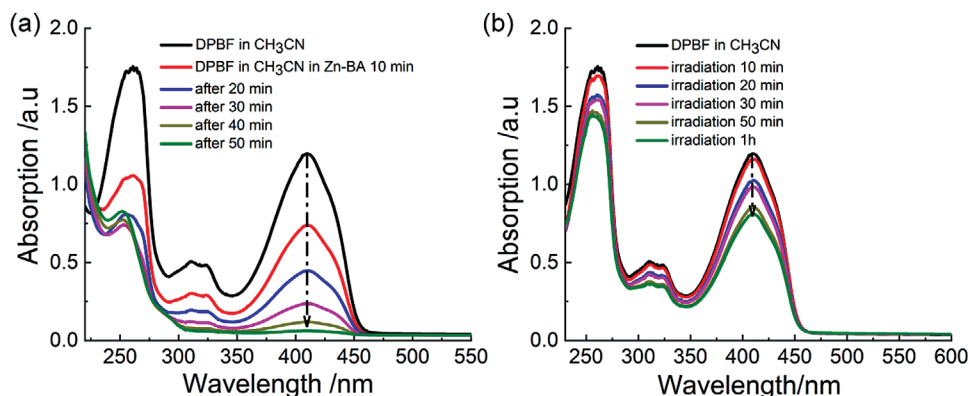


**Figure 4.** DPBF reactivity with  $^1\text{O}_2$  in acetonitrile a) using Zn-BA as a photosensitizer, b) without Zn-BA.

and  $1047\text{ cm}^{-1}$  corresponding to the  $-\text{O}-\text{O}-$ ,  $\text{C}-\text{O}-\text{C}$ , and  $-\text{C}-\text{O}-\text{C}-$  or  $\text{C}-\text{C sp}^3$ ,<sup>[41]</sup> respectively, as shown in Figure 3c. These new bands clearly reveal the formation of an endoperoxide species upon prolonged illumination with UV-light.

To confirm that the reaction involved reactive  $^1\text{O}_2$ , 1,3-diphenylisobenzofuran (DPBF) was used as a fluorescent probe for  $^1\text{O}_2$  (Figure S12, Supporting Information).<sup>[42–44]</sup> In acetonitrile, the DPBF absorption band at  $\approx 420\text{ nm}$  was found to linearly decrease upon irradiation with UV-light (365 nm) in the presence of Zn-BA SURMOF, and it completely vanishes within 50 min (Figure 4a). In the absence of Zn-BA, the rate of bleaching (420 nm band) is much slower, as can be seen in Figure 4b. These two experiments confirmed the role of  $^1\text{O}_2$  in the formation of endoperoxide-BA product.

In Zn-BA thin film, there are two possible mechanisms for the generation of reactive oxygen species, which form endoperoxide: i) photo-induced energy transfer to make  $^1\text{O}_2$  and ii) electron transfer, producing superoxide radical  $\text{O}_2^{\cdot-}$ . To confirm the exact mechanism, we performed EPR (electron paramagnetic resonance) spectroscopy employing two different spin traps, 2,2,6,6-tetramethyl-piperidine (TEMP) and 5,5-dimethyl-1-pyrroline-N-oxide (DMPO). TEMP traps  $^1\text{O}_2$  forming the persistent radical 2,2,6,6-Tetramethylpiperidine-1-oxyl (TEMPO),<sup>[45]</sup> and DMPO traps  $\text{O}_2^{\cdot-}$  forming the persistent radical DMPO-X (see Figure 5a).<sup>[46]</sup> We observed an EPR signal ( $g = 2.0056$ ,  $\text{AN} = 16.3\text{ G}$ )

only when TEMP was added in ambient conditions after UV-illumination, consistent with the reported EPR signal of TEMPO, confirming the generation of  $^1\text{O}_2$ .<sup>[47]</sup> In the control experiments, we did not observe a significant EPR signal of TEMPO in presence of Zn-BA SURMOF in dark. We also did not observe an EPR signal when DMPO was added both in dark and after illumination in presence of Zn-BA SURMOF (Figure 5b). These results indicate that  $^1\text{O}_2$  was only generated during illumination of Zn-BA SURMOF under ambient conditions. We thus conclude that the  $^1\text{O}_2$  is generated via energy transfer from photoexcited Zn-BA to  $^3\text{O}_2$ , and the  $^1\text{O}_2$  subsequently reacts with the BA to form endoperoxide species, without affecting the crystallinity (a topotactic transformation; Figure 5c). The crystallinity of the photoreacted Zn-BA MOF remains unaltered, because the photochemical change of the BA linker does not change the linker geometry.

### 3. Conclusion

A new photoactive MOF, Zn-BA, was synthesized using BA chromophore as a linker. Using a lbl, LPE process, it was possible to grow oriented, thin layers of the MOF, which exhibited an irreversible photochemical change upon prolonged UV-light illumination. Using the electronic and vibrational spectroscopy methods, NEXAFS and EPR, we could realize that the Zn-BA

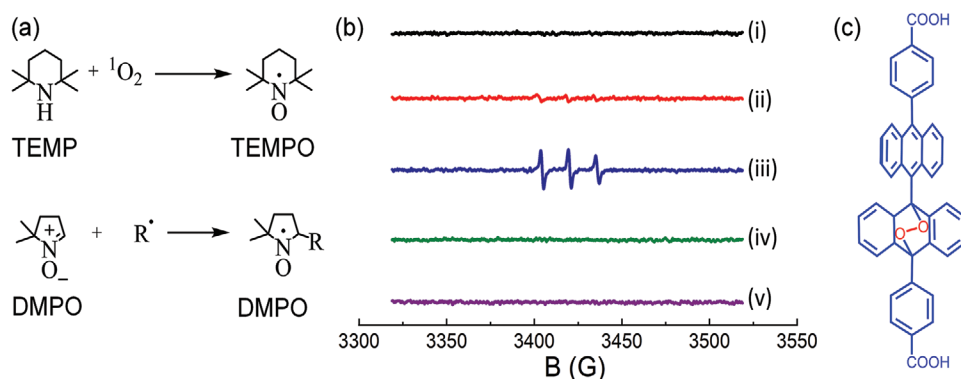


**Figure 5.** a) Reaction schemes of TEMP with  $^1\text{O}_2$  and DMPO with superoxide to produce persistent nitroxide radicals; b) EPR spectra: i) pristine Zn-BA, ii) TEMP dissolved in chloroform and methanol in presence of Zn-BA in dark and iii) after irradiation, iv) DMPO dissolved in chloroform in presence of Zn-BA in dark and v) after irradiation; c) postulated endoperoxide of BA linker.

MOF can sensitize reactive  $^1\text{O}_2$  at the ambient condition, and the generated  $^1\text{O}_2$  subsequently reacts to the one of the anthracene unit of the BA to form endoperoxide. This photochemical reaction in the periodic lattice of the MOF thin film is not affected by the solvent medium. Hence, to investigate photochemical conversions that are severely influenced by the solvent polarity, MOF structure can act as a potential template.

#### 4. Experimental Section

**Synthesis of Zn-BA SURMOF:** The Zn-BA SURMOF was synthesized using lbl, spin-coating, and spray-coating techniques as described in detail in previous works.<sup>[48,49]</sup> The functionalized substrates (precleaned quartz, Si/SiO<sub>2</sub>, and 11-mercapto-1-undecanol functionalized Au) were alternately spin coated (10 s, 1000 RPM) using 0.5 mL of ethanolic zinc acetate dihydrate ( $1 \times 10^{-3}$  M) and 0.5 mL of ethanolic BA ( $0.05 \times 10^{-3}$  M) linker solutions at room temperature. Between the metal and linker deposition, substrates were rinsed with 0.7 mL of pure ethanol to remove excess precursors. Linker synthesis is described in the supporting information (Figure S1–S5, Supporting Information)

**Electron Paramagnetic Resonance Spectroscopy:** Electron paramagnetic resonance (EPR) spectroscopy data were collected on a Bruker EMXNano spectrometer. All samples were measured in chloroform at 23 °C. The following parameters were used for the measurement, center field: 3428.7 G; sweep width: 200 G; sweep time: 30 s; sample g-factor: 2.0056; receiver gain: 40 dB; modulation amplitude: 1 G; number of scans: 3; microwave attenuation: 60 dB; number of points: 2000; modulation frequency: 100 kHz, modulation phase: 0; conversion time: 15 ms; time constant: 1.28 ms; points/modulation amplitude: 10.

The detection of singlet oxygen  $^1\text{O}_2$  was carried out by mixing 0.05 mL 2,2,6,6-tetramethyl-piperidine (TEMP) in 5 mL of methanol with 10 mL chloroform. After flushing the solution with O<sub>2</sub> for 5 min a pristine Zn-BA SURMOF was immersed in the liquid. Then, EPR was performed in the dark. Thereafter, the sample was irradiated with UV-light of 365 nm, followed by measuring the EPR signal after 1, 3, 6, 9 min, and 2 h irradiation.

To exclude that superoxide was produced, the following method was used. Pristine Zn-BA SURMOF was added to 10 mL chloroform followed by addition of 0.05 mL 5,5-dimethyl-1-pyrroline-N-oxide (DMPO). The reaction mixture was flushed for 5 min with O<sub>2</sub>. Subsequently, the EPR signal was recorded in the dark. Finally, the sample was irradiated with UV-light of 365 nm, followed by measuring the EPR signal after irradiation for 1, 3, 6, 9, and 15 min.

**X-Ray Diffraction:** The out-of-plane XRD measurements were carried out using a Bruker D8-Advance diffractometer equipped with a position-sensitive detector LynxEye operated with a variable divergence slit and a 2.3° Soller-slit on the secondary side. Cu K $\alpha_{1,2}$ -radiation ( $\lambda = 0.154018$  nm) was used in all cases. In-plane (non-co-planar orientation) XRD measurements were conducted on Bruker D8 Discover equipped with a quarter Eulerian cradle, tilt-stage and 2.3° Soller-slits were installed in both sides. A Göbel-mirror and a position sensitive detector Lynxeye in  $\theta$ - $2\theta$  geometry were applied in the measurement. The measurement was carried out in the range of  $2\theta = 2^\circ - 20^\circ$  at a scan step of 0.020° at 40 kV and 40 mA utilizing Cu K $\alpha_{1,2}$ -radiation ( $\lambda = 0.154018$  nm). The samples used for the XRD measurements were grown on Au-substrates.

**Infrared Reflection Absorption Spectroscopy:** The infrared reflection absorption spectroscopy (IRRAS) data were recorded using a Bruker Vertex 80 spectrometer purged with dried air. The IRRAS accessory (A518) has a fixed angle of incidence of 80°. The data were collected on a mid-band liquid nitrogen cooled MCT detector. Perdeuterated hexadecanethiolate-SAM on Au was used for reference measurements.

**UV-vis Spectroscopy:** UV-vis absorption spectra were recorded using an Agilent Cary 5000 UV-vis-NIR spectrophotometer, with the wavelength range of 200–600 nm in transmission mode.

**Attenuated Total Reflectance IR:** Attenuated total reflectance (ATR) measurements were conducted by Bruker Optics Tensor 27 spectrometer

equipped with platinum ATR (diamond crystal, 45°, one reflection) accessory and a deuterated L-alanine doped triglycine sulfate (LaDTGS) detector. The spectra were recorded at room temperature, with a resolution of 4 cm<sup>-1</sup>, and air is used to record the background.

**Raman Spectroscopy:** Raman spectroscopy was performed with a Bruker Senterra Raman microscope, equipped with a 50xOlympus MPLAN objective, NA 0.5, and a 532 nm-laser, operated at 200  $\mu\text{W}$  output power. For data acquisition and spectra analysis Bruker OPUS software 7.8 was used. For the Raman spectroscopy of the SURMOF, the spectra were recorded at five different positions on the sample and their intensities were averaged.

**NEXAFS Spectroscopy:** NEXAFS<sup>[50]</sup> experiments were carried out at the HE-SGM beamline at the synchrotron radiation facility BESSY II that is a part of the Helmholtz Zentrum Berlin (HZB). A moderate photon flux provided by this beamline is well suited for such radiation-sensitive samples. NEXAFS spectra were recorded at the carbon K-edge in partial electron yield (PEY) mode with retarding voltages of  $-150$  V. The linearly polarized synchrotron light with a polarization factor of  $\approx 91\%$  was used. The incidence angle of the X-rays was set to 55° in respect to the sample surface and the energy resolution was  $\approx 0.3$  eV.

#### Supporting Information

Supporting Information is available from the Wiley Online Library or from the author.

#### Acknowledgements

R.H. and C.W. acknowledged support from the Deutsche Forschungsgemeinschaft (DFG, German Research Foundation) under the Germany Excellence Strategy via the Excellence Cluster 3D Matter Made to Order (grant no. EXC-2082/1-390761711). The authors also thank HZB for the allocation of synchrotron radiation beam time at BESSY II. Z.M.H acknowledges the financial support of the Ministry of Higher Education of the Arab Republic of Egypt “MoHE”.

Open access funding enabled and organized by Projekt DEAL.

#### Conflict of Interest

The authors declare no conflict of interest.

#### Data Availability Statement

The data that support the findings of this study are available on request from the corresponding author. The data are not publicly available due to privacy or ethical restrictions.

#### Keywords

bianthryl, epitaxial thin films, metal–organic frameworks, singlet oxygen, topotactic reaction

Received: December 11, 2021

Revised: January 31, 2022

Published online:

[1] H. Furukawa, K. E. Cordova, M. O’Keeffe, O. M. Yaghi, *Science* **2013**, *341*, 1230444.

- [2] S. Kitagawa, R. Kitaura, S.-i. Noro, *Angew. Chem., Int. Ed.* **2004**, *43*, 2334.
- [3] H. Furukawa, Y. B. Go, N. Ko, Y. K. Park, F. J. Uribe-Romo, J. Kim, M. O'Keeffe, O. M. Yaghi, *Inorg. Chem.* **2011**, *50*, 9147.
- [4] B. Li, H.-M. Wen, W. Zhou, B. Chen, *J. Phys. Chem. Lett.* **2014**, *5*, 3468.
- [5] M. P. Suh, H. J. Park, T. K. Prasad, D.-W. Lim, *Chem. Rev.* **2012**, *112*, 782.
- [6] D. Yang, B. C. Gates, *ACS Catal.* **2019**, *9*, 1779.
- [7] L. E. Kreno, K. Leong, O. K. Farha, M. Allendorf, R. P. Van Duyne, J. T. Hupp, *Chem. Rev.* **2012**, *112*, 1105.
- [8] H.-Y. Li, S.-N. Zhao, S.-Q. Zang, J. Li, *Chem. Soc. Rev.* **2020**, *49*, 6364.
- [9] M. D. Allendorf, R. Dong, X. Feng, S. Kaskel, D. Matoga, V. Stavila, *Chem. Rev.* **2020**, *120*, 8581.
- [10] V. Stavila, A. A. Talin, M. D. Allendorf, *Chem. Soc. Rev.* **2014**, *43*, 5994.
- [11] S. Wuttke, D. D. Medina, J. M. Rotter, S. Begum, T. Stassin, R. Ameloot, M. Oschatz, M. Tsotsalas, *Adv. Funct. Mater.* **2018**, *28*, 1801545.
- [12] J. Liu, C. Wöll, *Chem. Soc. Rev.* **2017**, *46*, 5730.
- [13] R. Haldar, L. Heinke, C. Wöll, *Adv. Mater.* **2020**, *32*, 1905227.
- [14] C. R. Martin, P. Kittikhunnatham, G. A. Leith, A. A. Berseneva, K. C. Park, A. B. Greytak, N. B. Shustova, *Nano Res.* **2021**, *14*, 338.
- [15] M. Adams, M. Kozłowska, N. Baroni, M. Oldenburg, R. Ma, D. Busko, A. Turshatov, G. Emandi, M. O. Senge, R. Haldar, C. Wöll, G. U. Nienhaus, B. S. Richards, I. A. Howard, *ACS Appl. Mater. Interfaces* **2019**, *11*, 15688.
- [16] J. Liu, W. Zhou, J. Liu, I. Howard, G. Kilibarda, S. Schlabach, D. Coupry, M. Addicoat, S. Yoneda, Y. Tsutsui, T. Sakurai, S. Seki, Z. Wang, P. Lindemann, E. Redel, T. Heine, C. Wöll, *Angew. Chem., Int. Ed.* **2015**, *54*, 7441.
- [17] A. Aziz, A. R. Ruiz-Salvador, N. C. Hernández, S. Calero, S. Hamad, R. Grau-Crespo, *J. Mater. Chem. A* **2017**, *5*, 11894.
- [18] R. Haldar, Z. Fu, R. Joseph, D. Herrero, L. Martín-Gomis, B. S. Richards, I. A. Howard, A. Sastre-Santos, C. Wöll, *Chem. Sci.* **2020**, *11*, 7972.
- [19] S. De, T. Devic, A. Fateeva, *Dalton Trans.* **2021**, *50*, 1166.
- [20] R. Haldar, A. Mazel, M. Krstić, Q. Zhang, M. Jakoby, I. A. Howard, B. S. Richards, N. Jung, D. Jacquemin, S. Diring, W. Wenzel, F. Odobel, C. Wöll, *Nat. Commun.* **2019**, *10*, 2048.
- [21] R. Haldar, H. Chen, A. Mazel, D.-H. Chen, G. Gupta, N. Dua, S. Diring, F. Odobel, C. Wöll, *Adv. Mater. Interfaces* **2021**, *8*, 2100262.
- [22] B. Lü, Y. Chen, P. Li, B. Wang, K. Müllen, M. Yin, *Nat. Commun.* **2019**, *10*, 767.
- [23] R. Haldar, M. Kozłowska, M. Ganschow, S. Ghosh, M. Jakoby, H. Chen, F. Ghalami, W. Xie, S. Heidrich, Y. Tsutsui, J. Freudenberg, S. Seki, I. A. Howard, B. S. Richards, U. H. F. Bunz, M. Elstner, W. Wenzel, C. Wöll, *Chem. Sci.* **2021**, *12*, 4477.
- [24] P. I. Scheurle, A. Mähringer, A. C. Jakowetz, P. Hosseini, A. F. Richter, G. Wittstock, D. D. Medina, T. Bein, *Nanoscale* **2019**, *11*, 20949.
- [25] N. Sikdar, D. Dutta, R. Haldar, T. Ray, A. Hazra, A. J. Bhattacharyya, T. K. Maji, *J. Phys. Chem. C* **2016**, *120*, 13622.
- [26] C.-C. Chueh, C.-I. Chen, Y.-A. Su, H. Konnerth, Y.-J. Gu, C.-W. Kung, K. C. W. Wu, *J. Mater. Chem. A* **2019**, *7*, 17079.
- [27] R. Haldar, M. Jakoby, M. Kozłowska, M. Rahman Khan, H. Chen, Y. Pramudya, B. S. Richards, L. Heinke, W. Wenzel, F. Odobel, S. Diring, I. A. Howard, U. Lemmer, C. Wöll, *Chemistry – A European Journal* **2020**, *26*, 17016.
- [28] I. Roy, S. Goswami, R. M. Young, I. Schlesinger, M. R. Mian, A. E. Enciso, X. Zhang, J. E. Hornick, O. K. Farha, M. R. Wasielewski, J. T. Hupp, J. F. Stoddart, *J. Am. Chem. Soc.* **2021**, *143*, 5053.
- [29] R. Medishetty, J. K. Zaręba, D. Mayer, M. Samoć, R. A. Fischer, *Chem. Soc. Rev.* **2017**, *46*, 4976.
- [30] M. Adams, N. Baroni, M. Oldenburg, F. Kraffert, J. Behrends, R. W. MacQueen, R. Haldar, D. Busko, A. Turshatov, G. Emandi, M. O. Senge, C. Wöll, K. Lips, B. S. Richards, I. A. Howard, *Phys. Chem. Chem. Phys.* **2018**, *20*, 29142.
- [31] R. Haldar, S. Diring, P. K. Samanta, M. Muth, W. Clancy, A. Mazel, S. Schlabach, F. Kirschhöfer, G. Brenner-Weiß, S. K. Pati, F. Odobel, C. Wöll, *Angew. Chem., Int. Ed.* **2018**, *57*, 13662.
- [32] R. Medishetty, A. Husain, Z. Bai, T. Runčevski, R. E. Dinnebier, P. Naumov, J. J. Vittal, *Angew. Chem., Int. Ed.* **2014**, *53*, 5907.
- [33] X. Liu, A. Mazel, S. Marschner, Z. Fu, M. Muth, F. Kirschhöfer, G. Brenner-Weiss, S. Bräse, S. Diring, F. Odobel, R. Haldar, C. Wöll, *ACS Appl. Mater. Interfaces* **2021**.
- [34] R. Komskis, P. Adomėnas, O. Adomėnienė, P. Baronas, T. Serevičius, S. Juršėnas, *J. Phys. Chem. C* **2019**, *123*, 27344.
- [35] J. J. Piet, W. Schuddeboom, B. R. Wegewijs, F. C. Grozema, J. M. Warman, *J. Am. Chem. Soc.* **2001**, *123*, 5337.
- [36] J. K. Klosterman, M. Iwamura, T. Tahara, M. Fujita, *J. Am. Chem. Soc.* **2009**, *131*, 9478.
- [37] Z. Wang, L. Heinke, J. Jelic, M. Cakici, M. Dommaschk, R. J. Maurer, H. Oberhofer, S. Grosjean, R. Herges, S. Bräse, K. Reuter, C. Wöll, *Phys. Chem. Chem. Phys.* **2015**, *17*, 14582.
- [38] L. Heinke, M. Cakici, M. Dommaschk, S. Grosjean, R. Herges, S. Bräse, C. Wöll, *ACS Nano* **2014**, *8*, 1463.
- [39] J. Liu, B. Lukose, O. Shekhah, H. K. Arslan, P. Weidler, H. Gliemann, S. Bräse, S. Grosjean, A. Godt, X. Feng, K. Müllen, I.-B. Magdau, T. Heine, C. Wöll, *Sci. Rep.* **2012**, *2*, 921.
- [40] N. Sikdar, A. Hazra, D. Samanta, R. Haldar, T. K. Maji, *Angew. Chem., Int. Ed.* **2020**, *59*, 18479.
- [41] A. C. Ferrari, J. Robertson, A. C. Ferrari, J. Robertson, *Philosophical Transactions of the Royal Society of London. Series A: Mathematical, Physical and Engineering Sciences* **2004**, *362*, 2477.
- [42] X.-F. Zhang, X. Li, *J. Lumin.* **2011**, *131*, 2263.
- [43] M. Wozniak, F. Tanfani, E. Bertoli, G. Zolese, J. Antosiewicz, *Biochimica et Biophysica Acta (BBA) – Lipids and Lipid Metabolism* **1991**, *1082*, 94.
- [44] J. Park, Q. Jiang, D. Feng, H.-C. Zhou, *Angew. Chem., Int. Ed.* **2016**, *55*, 7188.
- [45] É. Hideg, C. Spetea, I. Vass, *Photosynth. Res.* **1994**, *39*, 191.
- [46] K. C. Das, H. P. Misra, *The Journal of biological chemistry* **1992**, *267*, 19172.
- [47] Z. Zhang, N. Wang, Q. Wan, M. Li, *Free Radical Biology and Medicine* **1993**, *14*, 1.
- [48] V. Chernikova, O. Shekhah, M. Eddaoudi, *ACS Appl. Mater. Interfaces* **2016**, *8*, 20459.
- [49] H. K. Arslan, O. Shekhah, J. Wohlgemuth, M. Franzreb, R. A. Fischer, C. Wöll, *Adv. Funct. Mater.* **2011**, *21*, 4228.
- [50] A. Nefedov, C. Wöll, in *Advanced Applications of NEXAFS Spectroscopy for Functionalized Surfaces*, (Eds.: G. Bracco, B. Holst), Springer, Berlin **2012**.